RSC Advances

PAPER

View Article Online
View Journal | View Issue

Cite this: *RSC Adv.*, 2022, **12**, 4224

Recovery of NH_4^+–N and PO_4^{3-}–P from urine using sludge-derived biochar as a fertilizer: performance and mechanism†

Chaoyang Yu *[ab]

Sludge-derived biochar (BS) was prepared by pyrolyzing municipal sludge at different temperatures and was used to recover NH_4^+–N and PO_4^{3-}–P from urine. The effects of dosage, adsorption time, and urine concentration on the adsorption of NH_4^+–N and PO_4^{3-}–P were investigated, and the adsorbed BS was used as a fertilizer to study its effect on the growth of pakchoi cabbage. The Elovich model was more consistent with the adsorption processes of NH_4^+–N and PO_4^{3-}–P. Both the NH_4^+–N and PO_4^{3-}–P adsorption isotherm model agreed with the Redlich–Peterson model. The Langmuir model showed that the largest adsorption capacity of BS600 for NH_4^+–N and PO_4^{3-}–P could reach 114.64 mg g^{-1} and 31.05 mg g^{-1}, respectively. The NH_4^+–N adsorption mechanism of BS may have complexation with O-containing functional groups and precipitation reactions, while the removal mechanism of PO_4^{3-}–P was co-precipitation. The pot experiment demonstrated that adsorbed BS600 can better promote the growth of pakchoi cabbage with the same amount of addition. With the addition of 5% adsorbed BS600, the weight of cabbage was 64.49 g heavier than without the addition of BS600. This research provided theoretical support for the recovery of NH_4^+–N and PO_4^{3-}–P from urine as a fertilizer.

Received 22nd November 2021
Accepted 15th January 2022

DOI: 10.1039/d1ra08558a

rsc.li/rsc-advances

1 Introduction

The rapid development of high-speed rail had brought convenient transportation for us, shortening people's travel time and making them more comfortable and convenient to travel. At the same time, it had also brought some problems. In the past, China's railway train toilet fecal sewage was directly discharged on the railway. However, the country paid more and more attention to the cause of environmental protection, and people had higher and higher requirements for the environment.[1] Since the opening of high-speed rail, passengers' fecal sewage had been collected by the toilet collector. With the development of the high-speed railroad, the amount of high-speed railway fecal sewage was also rapidly increasing.[2] According to the health department regulations, fecal sewage cannot be discharged directly along the railway line, and the sewage must be collected and then centralized. Hence, an economical and effective method to deal with high-speed railway fecal sewage was urgent.

The existing urine treatment methods mainly included chemical precipitation, electrochemical, adsorption, and membrane separation.[3–6] Among them, researchers had a great interest in the adsorption method to deal with urine because the adsorption method has the advantages of simple operation and high efficiency. Currently, there are also many materials used to treat urine, such as activated carbon, metal oxides, resins, and biochar.[7–11] Biochar has a strong ion exchange capacity, large specific surface area, and pore volume.[12,13] Besides, biochar is very stable owing to its aromatic structure. In recent years, many studies have shown that biochar has good adsorption properties for nitrogen and phosphorus.[14–16] The study showed that the maximum adsorption capacities of cassava straw biochar and banana straw biochar were 24.04 mg g^{-1} (NH_4^+–N) and 31.15 mg g^{-1} (PO_4^{3-}–P), respectively.[14] The adsorption capacity of NH_4^+–N and PO_4^{3-}–P was also improved by panda manure biochar (PMBC) modified by carboxymethyl cellulose (CMC) and nano zero-valent zinc (nZVZ), which could reach 40.31 mg g^{-1} (NH_4^+–N) and 154.30 mg g^{-1} (PO_4^{3-}–P), respectively.[17] Simultaneously, some scholars treated PO_4^{3-}–P in urine with α-Fe_2O_3 synergistic activated carbon, and most of the PO_4^{3-}–P in urine could be recovered.[7] Additionally, Mg–biochar was used for simultaneous P and N recovery from sewage sludge ash (SSA) and food wastewater (FW) using ground coffee bean (GCB) and palm tree trunk (PTT) waste. PTT Mg–biochar could recover 92.2% of PO_4^{3-}–P and 54.8% of NH_4^+–N, while GCB Mg–biochar could recover 79.5% of PO_4^{3-}–P and 38.6% of NH_4^+–N.[18] Notably, these modification methods were used to improve the NH_4^+–N and PO_4^{3-}–P adsorption capacity on the original biochar by introducing metal oxides. In contrast, sludge-derived biochar contained a large number of

[a]*College of Architecture and Environment, Sichuan University, Chengdu 610041, China. E-mail: wtu77_001@163.com*

[b]*Sichuan-Tibet Railway Co., Ltd., Chengdu 610041, China*

† Electronic supplementary information (ESI) available. See DOI: 10.1039/d1ra08558a

inorganic compounds (*e.g.*, Ca^{2+} and Mg^{2+}), which can effectively improve the NH_4^+–N and PO_4^{3-}–P adsorption capacity.[19,20]

In this study, sludge-derived biochar (BS) was prepared by pyrolyzing municipal sludge at different temperatures and recovered NH_4^+–N and PO_4^{3-}–P from urine. The objectives were to (1) investigate the effects of dosage, adsorption time, and urine concentration on the NH_4^+–N and PO_4^{3-}–P adsorption from the urine; (2) discuss the mechanism of NH_4^+–N and PO_4^{3-}–P adsorption in urine by sludge-derived biochar; (3) record the effect of adsorbed BS on the growth of pakchoi cabbage. This study provided a new method and theoretical support for the treatment and resource recovery of NH_4^+–N and PO_4^{3-}–P in urine.

2 Material and methods

2.1 Raw materials and reagents

Urine source: the experimental urine was fresh undiluted urine collected from healthy males. The concentrations of NH_4^+–N and PO_4^{3-}–P in urine were 450.0 ± 14.3 mg L^{-1} and 168.0 ± 7.2 mg L^{-1}, respectively, with a pH of 6.92 ± 0.3 and conductivity of (18.4 ± 1.8) mS cm^{-1}.

Reagents: amine molybdate (AR, Sinopharm Chemical Reagent Co., Ltd.) and nascent reagent (AR, Hash China). The water of the experiments was deionized water (DW).

2.2 Experimental materials

Preparation of sludge-derived biochar (BS): the dewatered municipal sludge was taken from a wastewater treatment plant in Chengdu (Sichuan Province, China), and a certain amount of sludge was dried in an oven at 90 °C to a constant weight. The dried sludge was crushed through a mortar and sieved through 80 mesh and the sieved sludge powder was collected. Then, the sludge powder was weighed into a crucible and compacted with a tight lid. The crucible was placed in a muffle furnace with a heating rate of 10 °C min^{-1} and pyrolyzed at different temperatures (300–600 °C) for 3 h. The black solid obtained from the crucible was biochar, and biochar was denoted as BS300, BS400, BS500, and BS600 depending on the pyrolysis temperature.

2.3 Adsorption experiment

25 mL of fresh urine was reacted in a 50 mL conical flask with a certain amount of adsorbent, and the conical flask was placed in a thermostatic shaker (IS-RDD3, Crystal Technology & Industries, Inc, USA) at 25 °C and 150 rpm for 24 h. After reaching the adsorption equilibrium, the supernatant was passed through a 0.45 μm nylon membrane and the remaining concentration of NH_4^+–N and PO_4^{3-}–P in the filtrate was analyzed. Three parallel experiments were performed for each group. The removal efficiency and adsorption capacity were calculated by eqn (1) and eqn (2), respectively.

$$R = \frac{C_0 - C_e}{C_0} \times 100\% \quad (1)$$

$$q_e = \frac{C_0 - C_e}{m} \times V \quad (2)$$

where R is the removal efficiency, %; C_0 is the concentration of NH_4^+–N and PO_4^{3-}–P in the initial solution, mg L^{-1}; C_e is the concentration of NH_4^+–N and PO_4^{3-}–P in the solution after adsorption equilibrium, mg L^{-1}; q_e is the adsorption capacity, mg g^{-1}; V is the solution volume, mL; m is the mass of adsorbent, mg.

2.3.1 Effect of dosage. 10–100 mg of adsorbent was added to 25 mL of urine and the experiments were performed in a constant temperature oscillator at 25 °C and 150 rpm for 24 h. The effect of the dosage on the adsorption of NH_4^+–N and PO_4^{3-}–P was investigated.

2.3.2 Adsorption kinetics. 60 mg of BS was added to 25 mL of urine and the experiments were performed in a constant temperature oscillator at 25 °C and 150 rpm for 5–1440 min. To investigate the adsorption process, the adsorption results were fitted with the pseudo-first order kinetic model (3), the pseudo-second order kinetic model (4), the Elovich model (5), and the intra-particle diffusion model (6).

$$q_t = q_e(1 - e^{-k_1 t}) \quad (3)$$

$$q_t = \frac{q_e^2 k_2 t}{1 + q_e k_2 t} \quad (4)$$

$$q_t = \frac{1}{\beta_E}\ln(\alpha_E \beta_E) + \frac{1}{\beta_E}\ln(t) \quad (5)$$

$$q_t = k_d t^{1/2} + C_i \quad (6)$$

where q_e and q_t are the adsorption capacity of adsorbent at adsorption equilibrium and time "t", mg g^{-1}, respectively; k_1 and k_2 are the pseudo-first order kinetic model constant and the pseudo-second order kinetic model constant, respectively; α_E is the initial adsorption rate, mg (g^{-1} min^{-1}); β_E is the surface coverage and activation energy related constant, g min^{-1}; k_d is the intra-particle diffusion model rate constant, and C_i is the boundary constant.

2.3.3 Adsorption isotherm. The concentrations of NH_4^+–N and PO_4^{3-}–P in fresh urine were diluted 0.8, 0.6, 0.5, 0.2, 0.1, 0.05 and 0.01 times, respectively. And then, the experiments were performed in a constant temperature oscillator at 25 °C and 150 rpm for 24 h. The adsorption isotherm data were fitted with the Langmuir model (7), Freundlich model (8), and Redlich–Peterson model (9) to analyze the adsorption mechanism.

$$q_e = \frac{q_m K_b C_e}{1 + K_b C_e} \quad (7)$$

$$q_e = K_f C_e^{1/n} \quad (8)$$

$$q_e = \frac{K_r C_e}{1 + a C_e^g} \quad (9)$$

where q_e is the adsorption capacity at equilibrium, mg g^{-1}; C_e is the concentration of NH_4^+–N and PO_4^{3-}–P at adsorption equilibrium; q_m is the theoretical maximum adsorption capacity

according to the Langmuir model, mg g^{-1}; K_b is the Langmuir model adsorption constant; K_f and n are the Freundlich equilibrium coefficient and dimensionless number, respectively; a and K_r are the constants of the Redlich–Peterson model, and g is between 0 and 1.

2.4 Pot experiment

The soil was taken from the campus of Sichuan University (Chengdu, Sichuan Province, China) and its basic properties are shown in Table S1.† The stones in the soil were removed before planting. The adsorbed BS was mixed with 1 kg soil in proportions (0%, 0.5%, 1%, 2%, and 5%) and then planted with pakchoi cabbage in the pots (10 cm in diameter and 15 cm in height). When the pakchoi cabbage was mature, the fresh weight and heavy metal content of the pakchoi cabbage were measured.

2.5 Detection method

Conductivity and pH were determined with a portable multi-parameter water quality analyzer (SX731, Shanghai San-Xin Instrumentation Factory, China); NH_4^+–N and PO_4^{3-}–P concentrations were determined with a double-beam UV spectrophotometer (TU-1901, Beijing Pu-analysis General Instrument Co., Ltd.). The specific surface area and pore volume were measured with a specific surface area and pore size analyzer (BET, Tristar II Plus 2.02, USA). The changes of functional groups of BS were analyzed using Fourier Transform Infrared Spectroscopy (FTIR, Nicolet-460, Thermo Fisher, USA). The crystalline structure and physical composition were analyzed using an X diffraction analyzer (XRD, D8X, Bruker, Germany). The surface morphological features and elemental composition were analyzed by Scanning Electron Microscopy with Energy Dispersive Spectroscopy (SEM-EDS, Zeiss SUPRA40, Germany). The elemental composition and valence state of biochars were analyzed using an X-ray photoelectron spectrometer (XPS, ESCALAB 250Xi, Thermo Fisher Scientific, USA). An elemental analyzer (Flash 2000, Thermo Fisher Scientific, USA) was used to determine C, H, O, and N contents. Heavy metals in the plants were determined by dry ashing-flame atomic absorption spectrophotometry.[21] The mixture was mixed with 1 g of biochar and 20 mL of DW at a solid–liquid ratio of 1 : 20. The pH of the mixture solution was determined with a pH meter (PHS-3C, Shanghai Rez, China), which was the pH of the BS. The ash content of the BS was determined by the scorching method.[22] Available P and NH_4^+–N of BS were measured by the colorimetric method.[23] The zeta potential of BS was determined at pH = 6.92 ± 0.3 using a potential analyzer (Nano-ZS90, Malvern, England). Leaching experiments were conducted on the soil after pot experiments using the acetic acid leaching method.[24]

3 Results and discussion

3.1 Characterization analysis

3.1.1 Physicochemical property analysis. The changes of C, H, N, and O contents in the sludge-derived biochar are shown in Table 1, and the contents of C, H, O, and N decreased with the increase of the pyrolysis temperature. The C content in BS decreased from 18.34% to 11.09% when the pyrolysis temperature increased from 300 °C to 600 °C. The contents of H and N in BS300 were 4.34% and 2.01%, respectively. However, the contents of H and N in BS600 were 1.69% and 0.67%, respectively. Notably, the content of O decreased from 23.68% to 12.17%. This result may be caused by the formation of volatile substances during pyrolysis, such as CO_2, CO, H_2O, and other types of hydrocarbons.[24] Notably, the content of Ca and Mg increased with the increase of pyrolysis temperature. The literature had shown that Ca and Mg were conducive to NH_4^+–N and PO_4^{3-}–P adsorption.[19,20] From Table 1, the H/C decreased with increasing pyrolysis temperature, which indicated that the stability of sludge-derived biochar was enhanced.[21] The decrease of the O/C ratio indicated that more aromatic carbon structures were generated in BS under higher temperature conditions.[14] The decrease of the O + N/C ratio from 3.301 to 1.767 suggested the decrease of N-containing functional groups.[14]

Table 1 Characteristics of sludge-derived biochar

	BS300	BS400	BS500	BS600
C (%)	18.34	16.84	13.49	11.09
H (%)	4.34	3.78	2.47	1.69
O (%)	23.68	19.70	15.33	12.17
N (%)	2.01	1.48	1.02	0.67
Ca (%)	10.38	13.98	17.19	19.35
Mg (%)	2.36	4.71	5.08	6.11
H/C	0.237	0.224	0.183	0.152
O/C	1.291	1.170	1.136	1.097
O + N/C	3.301	2.650	2.156	1.767
Ash (%)	51.63	58.2	67.69	74.38
pH	8.14	8.87	9.35	9.68
Specific surface area (m^2 g^{-1})	12.35	42.57	67.68	102.35
Pore volume (cm^3 g^{-1})	0.15	0.24	0.36	0.54
Proe size (nm)	14.35	16.51	17.69	27.21
NH_4^+–N (mg g^{-1})	1.237	0.394	0.085	0.033
Available-P (mg g^{-1})	0.581	0.426	0.409	0.398
Zeta potential (mV)	−8.67	−14.37	−19.36	−25.18

The increase in pyrolysis temperature from 300 °C to 600 °C increased the ash content by 22.75%. This phenomenon was caused by the high content of minerals in municipal sludge (*e.g.* silica and other inorganic compounds).[24,25] In addition, the increase in ash content was related to the decrease in C, H, O, and N content. This phenomenon was consistent with the results of many researchers.[21] The pH of the BS gradually increased with increasing pyrolysis temperature. The aliphatic compounds in the municipal sludge underwent condensation/polymerization reactions during pyrolysis and this reaction caused an increase of alkaline substances in the BS.[24,26]

The pore volume, specific surface area, and pore size of BS increased with the increase of pyrolysis temperature (Table 1). The pore volume, specific surface area, and pore size of sludge-derived biochar increased from 0.15 cm^3 g^{-1}, 12.35 m^2 g^{-1}, and 14.35 nm to 0.54 cm^3 g^{-1}, 102.35 m^2 g^{-1}, and 27.21 nm, respectively. It is suggested that high temperatures can expose more active sites to improve the removal ability of biochar.[27]

The literature showed that high temperature was able to produce more volatiles from sludge, and the richer pore structure on the biochar surface was produced.[28] It was also possible that the high temperature caused the original pore structure to collapse and form larger pores.[24] The content of NH_4^+–N and available-P in BS decreased from 1.237 mg g^{-1} and 0.581 mg g^{-1} to 0.033 mg g^{-1} and 0.398 mg g^{-1}, respectively, with the increase of pyrolysis temperature. The zeta potential of BS was all negative, which indicated that BS had a higher adsorption capacity for cations than for anions.[14,19,29]

The N_2 adsorption–desorption isotherm of BS belonged to type IV (Fig. 1a). When $P/P_0 < 0.4$, the gas entered into the pores, and the N_2 adsorption capacity increased sharply at this time. With the increase of P/P_0, the adsorption capacity gradually increased. At this time, the adsorption type of BS changed from single-molecular layer adsorption to multi-molecular layer adsorption, and multi-molecular layer adsorption was dominant. Moreover, adsorption–desorption curves in the second half of the isotherm did not overlap, which was caused by the multi-layer filling of capillary pores, indicating the existence of both micropores and mesopores in sludge-derived biochar.[17] The pore distribution (Fig. 1b) of the BS was mainly in the mesoporous range (2 nm < pore size < 50 nm).[17] The analysis of the N_2 adsorption–desorption isotherm and pore distribution indicated that the BS was a mesoporous material.

3.1.2 FTIR and XRD. The FTIR of sludge-derived biochar is shown in Fig. 1c. The peak of 3422 cm^{-1} was considered to be the stretching vibration of –OH. From Fig. 1c, the stretching vibration started to slowly weaken at the pyrolysis temperature from 300 to 600 °C, indicating that the related hydroxyl groups (–ROH and –COH) decomposed with the increase of the pyrolysis temperature.[30,31] The C=C/C=O structures were indicated by the vibrational peaks at 1620 cm^{-1} (BS300), 1624 cm^{-1} (BS400), 1628 cm^{-1} (BS500) and 1610 cm^{-1} (BS600).[26,32] The intensity of the C=C/C=O peak was the highest in BS600, indicating that BS600 was the most stable. The broad bands at 1402 cm^{-1}, 1400 cm^{-1}, 1492 cm^{-1}, and 1480 cm^{-1} corresponding to BS300, BS400, BS500, and BS600, respectively, were due to the stretching vibration of C=O/C–N.[33] The peak around 1043 cm^{-1} corresponded to the C–O stretching vibration, which became smaller and shifted to 1034 cm^{-1} as the pyrolysis temperature increased. The peak at 787 cm^{-1} represents the unsaturated alkane group (–CH–) in aromatic or isoaromatic compounds.[24] Notably, the peak of –CH– was still visible at 600 °C, indicating that the C in aromatic or heteroaromatic compounds was relatively stable.

The XRD analysis of the sludge-derived biochar is shown in Fig. 1d. The main component in the sludge-derived biochar was SiO_2,[24] followed by inorganic compounds containing Ca, mostly in the form of compounds containing Mg calcite and plagioclase zeolite.[24]

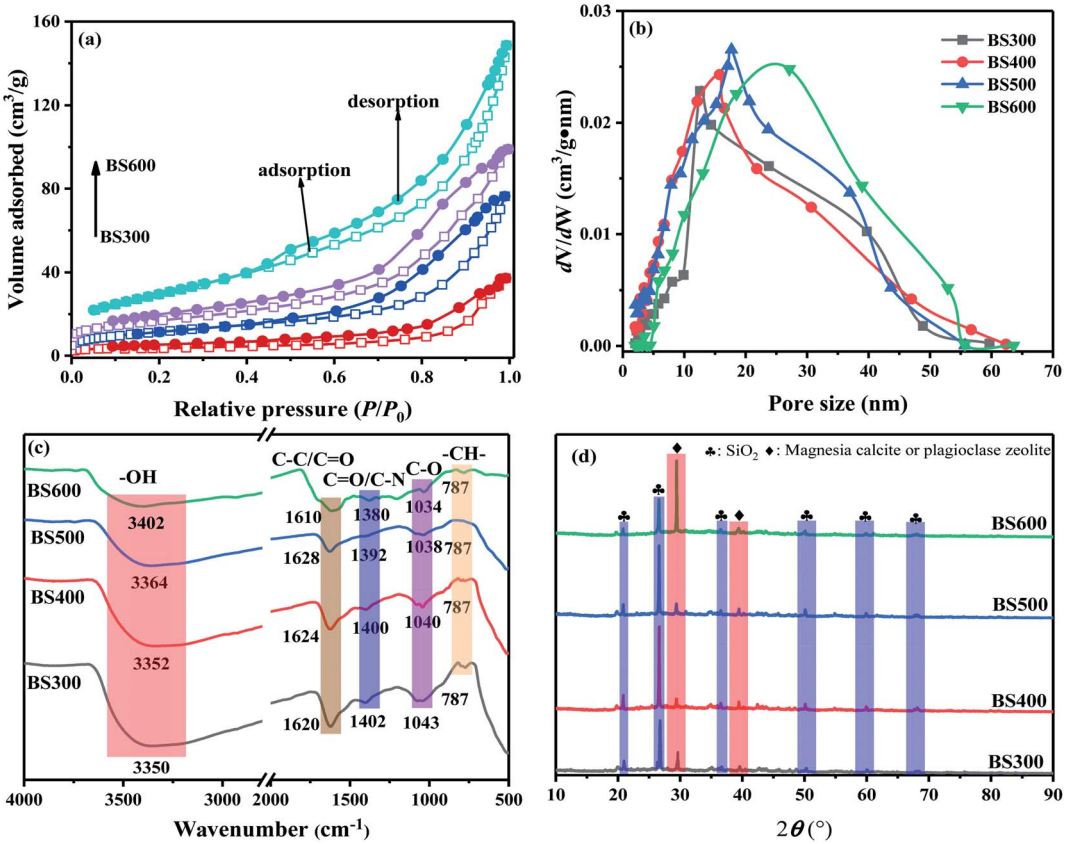

Fig. 1 N_2 adsorption and desorption (a); pore size distribution (b); FTIR (c) and XRD (d) characterization of sludge-derived biochar.

3.1.3 SEM-EDS. The morphological characteristics of the sludge-derived biochar are shown in Fig. 2. Rough and porous structures appeared on the surface of BS300 (Fig. 2a), indicating the presence of some highly conjugated aromatic compounds on the surface.[34] When the temperature was increased to 600 °C (Fig. 2d), a large number of porous structures with very rough and multi-grooved surfaces appeared. Furthermore, the EDS showed that the sludge-derived biochar contained inorganic substances (such as Ca and Mg). Notably, the content of Ca was much higher in BS600 than in other biochars.

3.1.4 XPS. The XPS analysis of the sludge-derived biochar is shown in Fig. 3. As shown in Fig. 3a, inorganic elements (such as Ca, Mg, and Si) can be observed in the overall spectrum. The peaks of Ca $2p_{3/2}$ and Ca $2p_{1/2}$ were presented in the fine spectrum of Ca 2p (Fig. 2b). The O 1s spectrum was divided into three peaks of O–H, C=O, and C–O.[34] As the pyrolysis temperature increased, the binding energy and relative content of the three peaks changed. The content of O–H and C–O decreased to 6.61% and 9.03%, respectively. However, the content of C=O increased from 26.35% to 84.36%. The C 1s spectrum was divided into three peaks of C–C/C–H, C–O, and C=O.[30] Notably, the binding energy of the C–C/C–H spectral peak (284.8 eV) has remained constant with the increase of the pyrolysis temperature, while the binding energies of C–O and C=O moved from 286.0 eV and 289.2 eV to 286.3 eV and 288.4 eV, respectively. And then, the relative contents of C–O and C=O changed from 33.45% and 10.52% to 17.46% and 15.07%, respectively. The relative content analysis of C–O and C=O illustrated that the content of C–O groups in BS decreased with increasing pyrolysis temperature, while the content of C=O increased with increasing temperature. This result was also consistent with the variation of C–O and C=O group contents in FTIR.

3.2 Effect of dosage on adsorption

The results of adsorbent dosage (10–100 mg L^{-1}) on the NH_4^+–N and PO_4^{3-}–P removal at a temperature of 25 °C and adsorption time of 24 h are shown in Fig. 4. When the dosage was increased from 10 mg to 60 mg, the removal efficiency of NH_4^+–N and PO_4^{3-}–P by BS gradually increased, presumably because the adsorption sites increased at the beginning with the increase of the dosage. The adsorption efficiency increased slowly when the dosage was greater than 60 mg, presumably because the increase in adsorbent content caused agglomeration among the adsorbents and thus reduced the number of adsorption sites, resulting in a slow increase in the removal efficiency.[7] Notably, the adsorption efficiency increased with increasing pyrolysis temperature, which was presumed to be related to its inorganic content, due to the reaction of inorganic substances (*e.g.* Ca or Mg) with NH_4^+–N and PO_4^{3-}–P to produce precipitation.[19] Therefore, 60 mg was chosen as the appropriate dosage for this experiment.

3.3 Adsorption kinetics

The effect of adsorption time on the NH_4^+–N and PO_4^{3-}–P removal at a temperature of 25 °C and dosage of 60 mg is shown in Fig. 5. Within 180 min, this process was a fast adsorption process for NH_4^+–N and PO_4^{3-}–P, and the adsorption capacity increased at a significant rate. In 180–600 min, the adsorbent adsorbed slowly, and then the adsorption reached equilibrium after 600 min. In the initial stage of adsorption, the adsorption rate was very fast due to the abundance of binding sites and pores on the adsorbent surface.[8,35] However, with the increase of time, the available binding sites and pores decreased, and then the adsorption gradually reached equilibrium. This phenomenon indicated that the reaction proceeded on the surface of the BS at the adsorption beginning. And then, the NH_4^+–N and PO_4^{3-}–P gradually penetrated from the surface to the inner surface of the BS, which led to a slower adsorption rate owing to the active sites on the inner surface being less than those on the outer surface.[29,36]

To evaluate the adsorption characteristics of BS on NH_4^+–N and PO_4^{3-}–P, the pseudo-first order kinetic model, the pseudo-second order kinetic model, the Elovich model, and the intra-particle diffusion model were applied to the adsorption data, and the results are shown in Fig. 5 and Table 2. By comparing the correlation coefficients R^2 of the pseudo-first order kinetic model and the pseudo-second order kinetic model, the result showed that the pseudo-second order kinetic model could

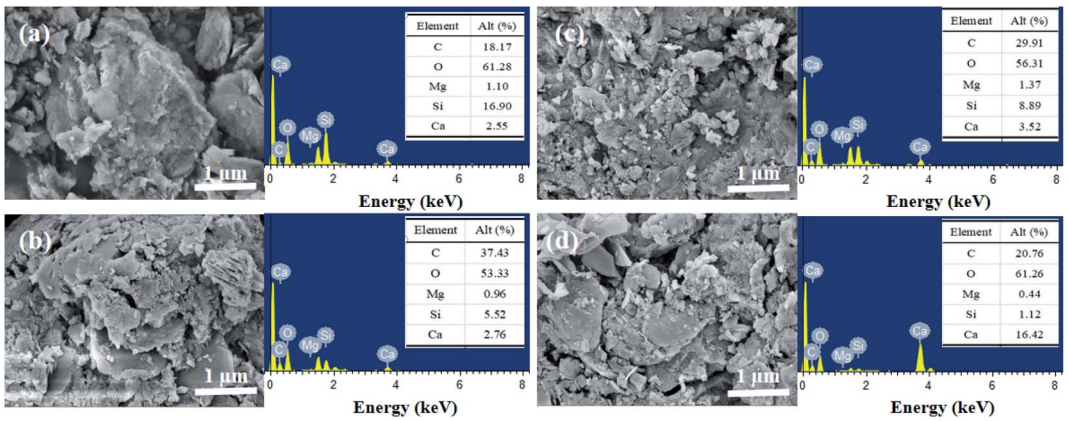

Fig. 2 SEM-EDS analysis of sludge-derived biochar ((a) BS300; (b) BS400; (c) BS500; and (d) BS600).

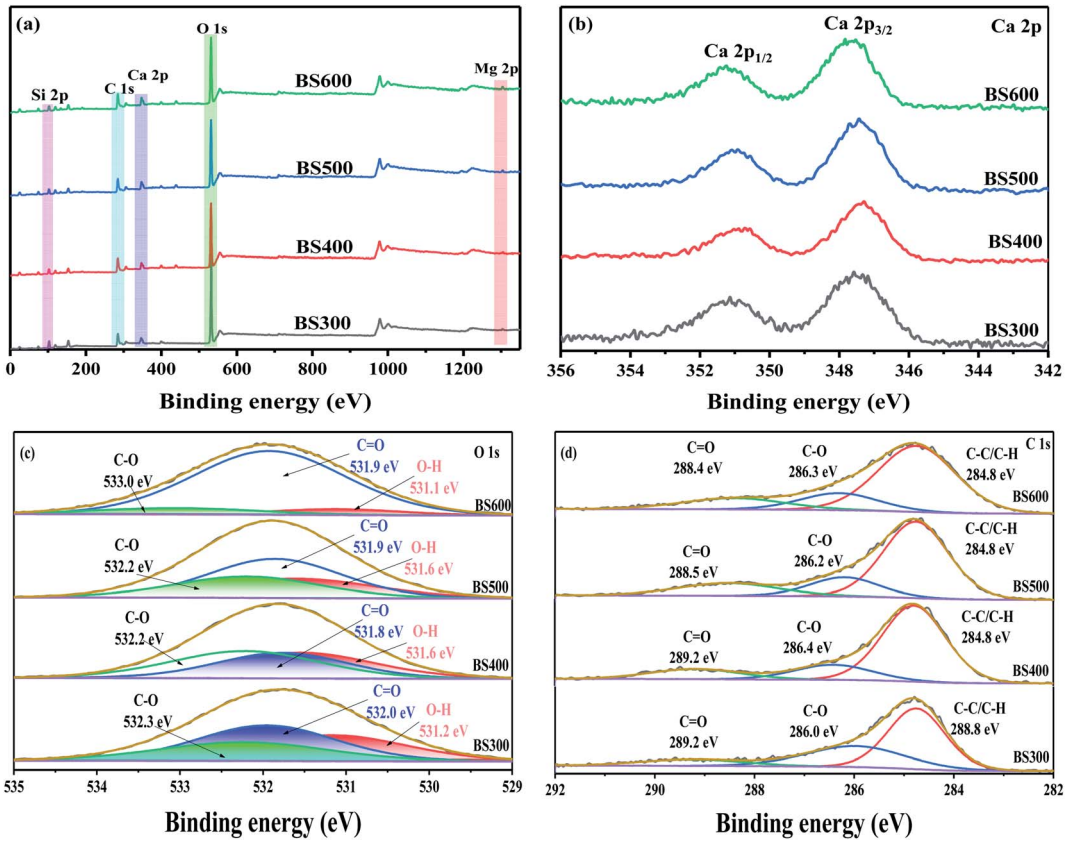

Fig. 3 XPS analysis of sludge-derived biochar ((a) full-spectrum, (b) Ca 2p, (c) O 1s and (d) C 1s).

better describe the kinetic processes of NH_4^+–N and PO_4^{3-}–P adsorption by BS, suggesting that the adsorption process was dominated by chemisorption.[7,34,37,38] In addition, the pseudo-second order model constant k_2 increased with the increase of pyrolysis temperature, which was presumed to be due to the formation of a richer pore structure on the surface of the biochar, thus exposing more adsorption sites.[35] The correlation coefficient R^2 of the Elovich model can reach above 0.95, indicating that the adsorption processes were mainly influenced by chemisorption, and the activation energy varies greatly.[7] Moreover, this result indicated that the adsorption process was multilayer adsorption on an inhomogeneous interface, including not only its diffusion at the adsorbent interface but also the activation and de-activation of the surface.[7,9,37]

The kinetics data were fitted by the intra-particle diffusion model, and the results are displayed in Fig. S1 and Table S2.† The fitting analysis of the intraparticle diffusion model revealed that the adsorption process can be divided into three stages. In the first stage of diffusion, the adsorbate was adsorbed from the aqueous phase to the outer surface of the adsorbent.[7,26] At this time, the mass transfer resistance was small, and the adsorption rate was fast. Subsequently, the available adsorption sites on the outer surface of BS decreased and the adsorption process entered the second stage.[7,9] At this point, the NH_4^+–N and PO_4^{3-}–P entered the inner pore of BS and the adsorption rate

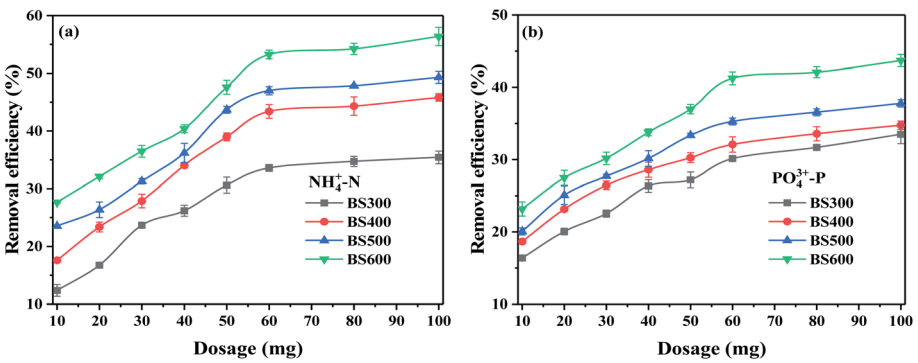

Fig. 4 Effect of sludge-derived biochar dosing on the removal of NH_4^+–N (a) and PO_4^{3-}–P (b).

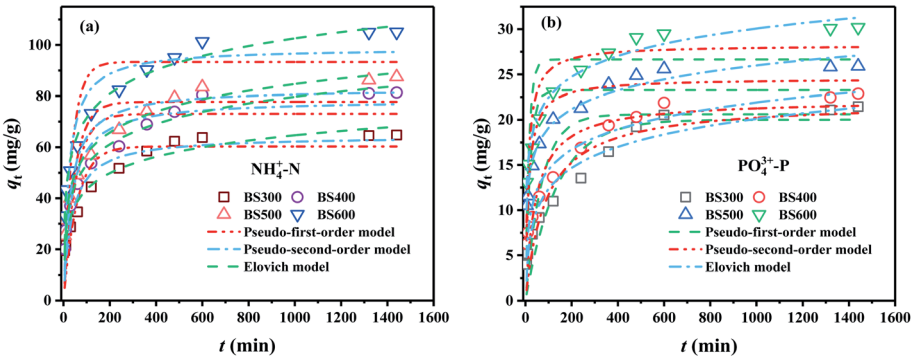

Fig. 5 Adsorption kinetics of sludge-derived biochar for NH_4^+–N (a) and PO_4^{3-}–P (b) removal.

became slower. Finally, the adsorption reached the third stage of adsorption–desorption dynamic equilibrium. In addition, the fitted straight line did not pass through the origin, indicating that the adsorption process was controlled by the boundary layer to some extent, and the intra-particle diffusion was not the only rate-limiting step.[7,26] From Table S2,† the intra-particle diffusion rate constants $k_{d1} > k_{d2} > k_{d3}$ and the boundary layer constants $C_1 < C_2 < C_3$ indicated that the first stage played a dominant role, which was because the BS can provide a large number of available active sites in the initial stage.[35] After the surface available active sites were gradually saturated, the NH_4^+–N and PO_4^{3-}–P adsorption was mainly controlled by the intra-particle diffusion rate.

3.4 Adsorption isotherm

The effect of fresh urine at different dilution levels on the NH_4^+–N and PO_4^{3-}–P removal was investigated at the adsorption temperature of 25 °C, the dosage of 60 mg, and the adsorption time of 24 h. The results are shown in Fig. 6. The adsorption capacity of NH_4^+–N and PO_4^{3-}–P increased rapidly, and then the trend of increasing adsorption decreased. Notably, the adsorption capacity of NH_4^+–N and PO_4^{3-}–P by BS increased with the increase of pyrolysis temperature.

The results were fitted by the Langmuir model, Freundlich model, and Redlich–Peterson model as shown in Fig. 6 and Table 3. The Langmuir model, Freundlich model, and Redlich–Peterson adsorption isotherm model can well describe the adsorption process ($R^2 > 0.9$), confirming that the NH_4^+–N and PO_4^{3-}–P adsorption process on BS was a combination of monolayer and multilayer adsorption.[19,34] Nevertheless, the R^2 of the Redlich–Peterson model was higher, showing that the Redlich–Peterson model can better describe the adsorption process of NH_4^+–N and PO_4^{3-}–P by BS. These results also confirmed that the adsorption process of NH_4^+–N and PO_4^{3-}–P belonged to a combination of multiple mechanisms.[38,39] The characteristic coefficient K_b in the Langmuir model was correlated with the adsorption performance. The value of K_b increased with the increase of BS pyrolysis temperature in this experiment, which also confirmed that the high-temperature pyrolysis was favorable for the adsorption of NH_4^+–N and PO_4^{3-}–P by BS.[40] The NH_4^+–N and PO_4^{3-}–P adsorption capacity by sludge-derived biochar increased with the increase of pyrolysis temperature, which also indicated that higher pyrolysis temperature was beneficial to the adsorption.[29] Simultaneously, the maximum adsorption of NH_4^+–N and PO_4^{3-}–P by BS600 was 114.71 mg g^{-1} and 30.29 mg g^{-1}, respectively. This also suggested that higher pyrolysis temperatures were beneficial to the recovery of NH_4^+–N and PO_4^{3-}–P from urine by BS. This result was considered to be that high-temperature pyrolysis can produce larger specific surface area and wider pore structure and provide more active sites; thus, the H_4^+–N and PO_4^{3-}–P adsorption capacity by BS was improved.[41] The $1/n$ in the Freundlich model was less than 1, indicating that the NH_4^+–N and PO_4^{3-}–P adsorption was easy to occur.[35] Comparing the adsorption capacity of different types of adsorption for NH_4^+–N and PO_4^{3-}–P (Table S3†), the adsorption capacity of BS600 for NH_4^+–N was much higher than that of other types of adsorbents. However, the adsorption capacity of BS600 for PO_4^{3-}–P

Table 2 Adsorption kinetic fitting parameters

		Pseudo-first-order			Pseudo-second-order			Elovich		
		q_m	k_1	R^2	q_m	k_2	R^2	α	β	R^2
NH_4^+–N	BS300	60.30	0.017	0.821	64.42	3.34×10^{-4}	0.910	10.31	0.109	0.967
	BS400	73.06	0.020	0.811	78.63	3.71×10^{-4}	0.914	11.55	0.087	0.983
	BS500	77.72	0.021	0.770	83.02	4.01×10^{-4}	0.890	15.73	0.085	0.985
	BS600	93.32	0.027	0.725	98.78	4.44×10^{-4}	0.869	27.28	0.074	0.986
PO_4^{3-}–P	BS300	20.00	0.007	0.866	22.01	0.52×10^{-3}	0.924	1.31	0.296	0.953
	BS400	20.60	0.014	0.791	22.20	1.02×10^{-3}	0.888	2.88	0.310	0.969
	BS500	23.27	0.049	0.692	24.55	3.03×10^{-3}	0.869	17.40	0.333	0.979
	BS600	26.64	0.065	0.603	28.23	3.14×10^{-3}	0.820	29.02	0.302	0.979

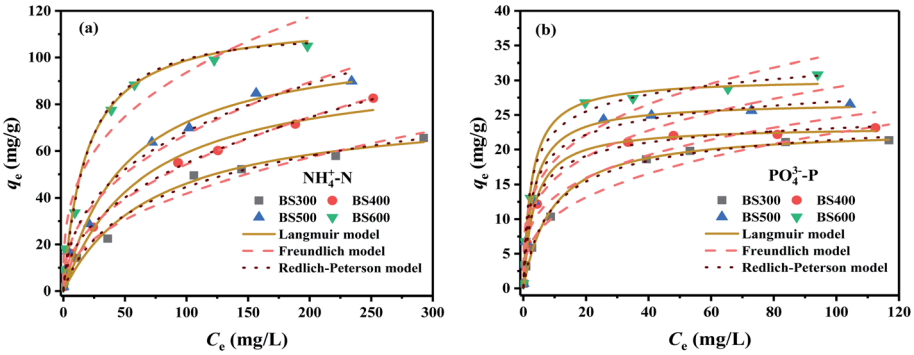

Fig. 6 Adsorption isotherms for NH_4^+–N (a) and PO_4^{3-}–P (b) removal by sludge-derived biochar.

was lower than that of bamboo leaf biochar and panda manure biochar. This may be caused by the lower concentration of PO_4^{3-}–P in urine and the negatively charged surface of biochar.[20,29] It may also be caused by the difference in raw materials of biochar.[19] However, sludge-derived biochar was also capable of being an excellent NH_4^+–N and PO_4^{3-}–P adsorbent.

The literature has reported that PO_4^{3-}–P adsorption was not favored under weakly acidic or alkaline conditions.[14] The reason speculated that the surface of sludge-derived biochar was negatively charged and generated electrostatic repulsion with PO_4^{3-}–P, which reduced the adsorption of phosphate.[7,10] In this work, the main reason for PO_4^{3-}–P adsorption was the release of Ca^{2+} from the sludge-derived biochar into the solution to react with PO_4^{3-}–P to form a precipitate (eqn (10)).[26,42] And the NH_4^+–N adsorption might be related to the complexation reaction of O-containing functional groups in the BS and the precipitation reaction with inorganic substances.[7,43,44] Many researchers had shown that NH_4^+, PO_4^{3-} combined with Mg^{2+} to form struvite (eqn (11)), which was presumed to be the main mechanism for the decrease in NH_4^+–N and PO_4^{3-}–P concentrations in urine.[39,41,45] Adsorption and co-precipitation were presumed to be the mechanisms for the decrease in urinary NH_4^+–N and PO_4^{3-}–P concentrations.

$$3PO_4^{3-} + 5Ca^{2+} + OH^- \rightleftharpoons Ca_5(OH)(PO_4)_3 \downarrow (pK_s = 57.5, 25\ ^\circ C) \quad (10)$$

$$Mg^{2+} + PO_4^{3-} + NH_4^+ + 6H_2O \rightarrow MgNH_4PO_4 \cdot 6H_2O \downarrow (pK_s = 12.6, 25\ ^\circ C) \quad (11)$$

3.5 Adsorption mechanism

The FTIR of BS600 before and after adsorption of NH_4^+–N and PO_4^{3-}–P is shown in Fig. S2a.† The peak at 3402 cm^{-1} was attributed to the stretching vibration of –OH, and the wave peak was enhanced and shifted to 3422 cm^{-1} after adsorption, indicating that –OH was involved in the adsorption of NH_4^+–N and PO_4^{3-}–P.[12,14,38] Meanwhile, the vibrational peak of C–C/C–O at the wavenumber of 1610 cm^{-1} after adsorption was shifted to 1642 cm^{-1}, which indicated that the C–C/C–O group was involved in the adsorption of NH_4^+–N and PO_4^{3-}–P.[14,30,46] The characteristic peak of phosphate was found at 1041 cm^{-1}, and the wave peak was sharper after adsorption, indicating that BS600 successfully adsorbed PO_4^{3-}–P.[14,30,47] Meanwhile, a new peak appeared at 1428 cm^{-1}, attributed to the stretching vibration peak of N–H.[9,44] In summary, –OH and C–C/C–O played an important role in the adsorption of NH_4^+–N and PO_4^{3-}–P by BS.

The strong diffraction peaks at 2θ 14.98°, 15.82°, 16.50°, 20.10°, 30.63°, 31.80°, 33.28°, and 33.69° indicated that BS600 combined with NH_4^+–N and PO_4^{3-}–P in urine to form granite crystals (Fig. S2b†).[12,14,22,32,47] A new diffraction peak appeared at 2θ of 38.71°, which was considered as $Ca_5(OH)(PO_4)_3$ precipitation, suggesting that Ca reacted with $PO3_4^{3-}$–P in BS600 to form a precipitate.[46] The above analysis indicated that co-

Table 3 Parameters of adsorption isotherm fitting

		BS300		BS400		BS500		BS600	
Model		NH_4^+–N	PO_4^{3-}–P	NH_4^+–N	PO_4^{3-}–P	NH_4^+–N	PO_4^{3-}–P	NH_4^+–N	PO_4^{3-}–P
Langmuir	K_b	0.014	0.108	0.015	0.292	0.020	0.323	0.054	0.387
	Q_{max}	79.64	23.13	97.60	23.38	109.16	26.90	114.71	30.29
	R^2	0.986	0.993	0.980	0.993	0.982	0.986	0.985	0.988
Freundlich	K_f	5.245	4.85	6.57	7.08	9.83	8.55	20.21	10.08
	n	2.22	3.01	2.18	3.70	2.40	3.77	3.05	3.81
	R^2	0.982	0.962	0.998	0.944	0.986	0.942	0.956	0.952
Redlich–Peterson	K_r	1.71	2.99	15.98	8.78	11.27	12.67	6.757	16.67
	a	0.072	0.176	1.993	0.497	0.753	0.660	0.069	0.769
	g	0.797	0.934	0.575	0.936	0.657	0.922	0.969	0.919
	R^2	0.988	0.995	0.999	0.996	0.988	0.991	0.987	0.993

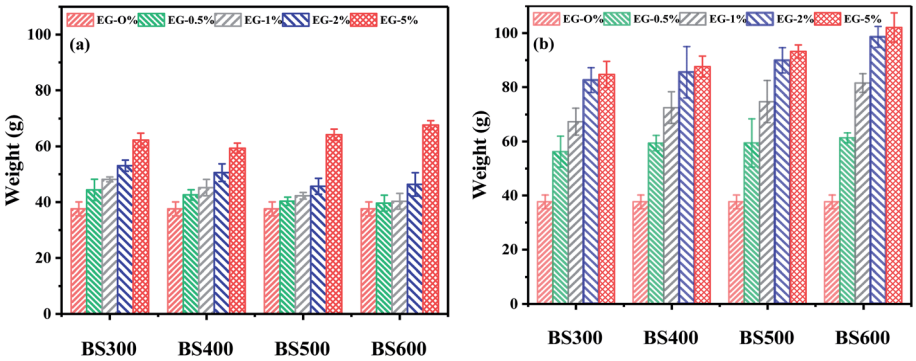

Fig. 7 Effect of sludge-derived biochar (a) and adsorbed sludge-derived biochar (b) dosing on the fresh weight of pakchoi cabbage.

precipitation was the main mechanism for the removal of NH_4^+–N and PO_4^{3-}–P from urine by BS.

In summary, the mechanism of NH_4^+–N and PO_4^{3-}–P adsorption in urine by BS may include co-precipitation, in which the main role was played by the generation of granite crystalline precipitation. In addition, NH_4^+–N also complexed with the O-containing functional group on BS.

3.6 Pot experiments

As shown in Fig. 7, the fresh weight of pakchoi cabbage showed an increasing trend when the addition amount of BS was gradually increased from 0% to 5%. The fresh weight of pakchoi cabbage increased significantly when the addition amount was increased from 0% to 2%, whereas the fresh weight of pakchoi cabbage increased greatly at the addition amounts of 2% and 5%. When no BS was added, the fresh weight of pakchoi cabbage was 37.57 g. However, when unadsorbed BS was added, the fresh weight of pakchoi cabbage was all enhanced. Notably, BS after adsorption can improve the fresh weight of pakchoi cabbage better than BS. Additionally, the highest fresh weight of pakchoi cabbage was obtained by adding adsorbed BS600 at the same addition amount, presumably due to the ability of BS600 to adsorb more NH_4^+–N and PO_4^{3-}–P in the urine. The addition of 5% adsorbed BS600 made the weight of pakchoi cabbage 64.49 higher than that of no BS600, indicating that the adsorbed BS was effective in promoting the growth of pakchoi cabbage.

Meanwhile, the Pb, Cr, Cd, As, Ni, Zn, and Cu contents in pakchoi cabbage were also analyzed (Table S4†). The heavy metal contents of Pb, Cr, Cd, As, Ni, Zn, and Cu in pakchoi cabbage were lower than the limit value (Standard for the Detection of Heavy Metal Contents in Vegetables), which indicated that the sludge-derived biochar could effectively become a source of fertilizer for vegetables after adsorption of NH_4^+–N and PO_4^{3-}–P from urine, and also provided a basis for the reuse of resources. In addition, the soil in the pot experiment was analyzed for leaching experiments (Table S5†). The results showed that the leaching concentrations of heavy metals in the soil were much lower than the leaching toxicity identification criteria values, which confirmed the feasibility of BS for the recovery of NH_4^+–N and PO_4^{3-}–P from urine as a fertilizer.

In this paper, sludge-derived biochar was prepared by pyrolysis of municipal sludge at different temperatures and applied to recover N and P from urine. The results showed that the maximum adsorption of NH_4^+–N and PO_4^{3-}–P by BS600 could reach 114.71 mg g^{-1} and 30.29 mg g^{-1}, respectively. In addition, the heavy metal content of chard was analyzed separately, and the results showed that the concentrations of many heavy metals were very low. Then, the leaching experiments were performed on the soil after planting, and the results showed that the heavy metal leaching concentrations were all within the standard range. The above analysis showed that the adsorbed sludge-derived biochar could be a potential fertilizer. It also provided a new idea for the treatment of municipal sludge and high-speed railway fecal sewage.

4 Conclusion

Sludge-derived biochar (BS) was prepared by pyrolysis of municipal sludge and used for NH_4^+–N and PO_4^{3-}–P adsorption from urine. Kinetic studies showed that the adsorption of both NH_4^+–N and PO_4^{3-}–P could reach adsorption equilibrium within 12 h, and the kinetic adsorption was more consistent with the Elovich model, which was multilayer adsorption at inhomogeneous interfaces and controlled by multiple diffusion rates during the adsorption process. The adsorption isothermal model of both NH_4^+–N and PO_4^{3-}–P was consistent with the Redlich–Peterson model, which indicated that the adsorption was a combination of monolayer adsorption and multilayer adsorption. The maximum adsorption of BS600 for NH_4^+–N and PO_4^{3-}–P could reach 114.71 mg g^{-1} and 30.29 mg g^{-1}, respectively. The adsorption mechanism of BS on NH_4^+–N may have complexation with O-containing functional groups and precipitation reactions, while the removal mechanism of PO_4^{3-}–P was co-precipitation. Simultaneously, the addition of adsorbed BS600 at 5% can better promote the growth of pakchoi cabbage. This work presented a new way and basis for resource utilization and recycling of municipal sludge and urine.

Ethical statement

All experiments were performed in accordance with the ethical guidelines, and approved by the ethics committee at Sichuan university. Informed consents were obtained from human participants of this study.

Funding

This work was supported by National Key R&D Program (2018YFC1505404) and Sichuan Provincial Science and Technology Department Science and Technology Plan Project (No. 2021YJ0033).

Conflicts of interest

The authors declare that they have no competing financial interests.

References

1 W. M. Chen and Y. X. Zheng, *Railway Stand. Des.*, 2012, **9**, 123–126.
2 M. Hu, B. Fan, B. Qu and S. K. Zhu, *China Water Wastewater*, 2016, **32**, 20–26.
3 Y. Gao, W. Zhang, B. Gao, W. Jia, A. Miao, L. Xiao and L. Yang, *Water Res.*, 2018, **139**, 301–310.
4 Y. J. Dai, W. Wang, L. Lu, L. Yan and D. Yu, *J. Cleaner Prod.*, 2020, **257**, 120573.
5 Q. Q. Yin, Z. B. Dong, R. K. Wang and Z. H. Zhao, *Environ. Sci. Pollut. Res.*, 2017, **24**, 26297–26309.
6 Z. Zeng, S. D. Zhang, T. Q. Li, F. L. Zhao and M. T. Rafiq, *J. Zhejiang Univ., Sci., B*, 2013, **14**, 1152–1161.
7 Y. Y. Jiao, S. K. Zhou, L. C. Zhang, W. D. Ai, S. Kang, C. L. Li, L. B. Zheng and Y. S. Wei, *Chem. Ind. Eng. Prog.*, 2021, **40**, 2347–2356.
8 X. T. Jiang and J. Chi, *J. Agric. Environ. Sci.*, 2014, **33**, 1817–1822.
9 Y. H. Jiang, L. I. An-Yu, F. Yan and H. Deng, *J. Agric. Resour. Environ.*, 2018, **35**, 559–567.
10 W. D. Wang, H. Liu, Y. T. Zhang and S. J. Yang, *Environ. Sci.*, 2016, **37**, 3186–3191.
11 J. J. Xu, X. H. Wu, N. W. Zhu, Y. W. Shen and H. P. Yuan, *Sci. Total Environ.*, 2020, **748**, 141367.
12 M. Yi, T. T. Li, H. H. Li, H. Qiao and Z. M. Yang, *Environ. Sci.*, 2019, **40**, 1318–1327.
13 L. F. Yue, Y. Xie, L. Shi, X. L. Li, F. R. Li and J. F. Wang, *Chin. J. Environ. Eng.*, 2015, **9**, 1221–1226.
14 Y. H. Jiang, A. Y. Hua, H. Deng, C. H. Ye, Y. Q. Wu, Y. D. Linmu and H. L. Hang, *Bioresour. Technol.*, 2019, **276**, 183–189.
15 S. H. Mood, M. Ayiania, H. L. Cao, O. Marin-Flores and M. Garcia-Perez, *Biomass Convers. Biorefin.*, 2021, **14**, 1–20.
16 Y. Gao, C. Yan, R. Wei, W. Zhang and L. Yang, *Ecol. Eng.*, 2019, **138**, 71–78.
17 M. J. Wang, S. K. Hu, Q. G. Wang, Y. Liang, C. R. Liu, H. Xu and Q. Ye, *J. Cleaner Prod.*, 2020, **291**, 125221.
18 M. Zin and D. J. Kim, *J. Hazard. Mater.*, 2020, **403**, 123704.
19 W. F. Cheng, H. Li, Y. Q. Yang, B. Yin and H. B. Liu, *CIESC J.*, 2016, **67**, 1541–1548.
20 L. Zhang, F. Deng, Z. K. Liu and L. X. Ai, *J. Environ. Manage.*, 2021, **282**, 111970.
21 Z. Khanmohammadi, M. Afyuni and M. R. Mosaddeghi, *Waste Manage. Res.*, 2015, **33**, 275.
22 A. D. Abdelhafid, S. X. Chang, Y. S. Ok, A. U. Rajapaksha and A. Anyia, *Environ. Sci. Pollut. Res.*, 2018, **25**, 25799–25812.
23 M. K. Hossain, V. Strezov, K. Y. Chan, A. Ziolkowski and P. F. Nelson, *J. Environ. Manage.*, 2011, **97**, 223–228.
24 J. W. Jin, Y. A. Li, J. Y. Zhang, S. C. Wu, Y. C. Cao, P. Liang, J. Zhang, M. H. Wong, M. Y. Wang and S. D. Shan, *J. Hazard. Mater.*, 2016, **320**, 417–426.
25 T. Chen, Z. Y. Zhou, H. Rong, R. H. Meng, H. T. Wang and W. J. Lu, *Chemosphere*, 2015, **134**, 286–293.
26 M. Chen, F. Wang, D. L. Zhang and W. M. Yi, *Environ. Sci.*, 2019, **40**, 5421–5429.
27 T. Chen, Z. Y. Zhou, X. Sai, H. T. Wang and W. J. Lu, *Bioresour. Technol.*, 2015, **190**, 388–394.
28 T. Chen, Z. Zhou, R. Han, R. Meng, H. Wang and W. Lu, *Chemosphere*, 2015, **134**, 286–293.
29 X. Liu, H. Y. Nan and Q. An, *J. Agric. Resour. Environ.*, 2017, **35**, 66–73.
30 A. Y. Li, S. L. Li, B. G. Yu, A. Y. Ma, X. L. Zhou, J. H. Xie, Y. H. Jiang and H. Deng, *CIESC J.*, 2020, **71**, 1683–1695.
31 Y. H. Du, E. C. Jiang, Z. Y. Li, S. J. Zhang and M. F. Wang, *Trans. Chin. Soc. Agric. Mach.*, 2016, **47**, 193–199+214.
32 N. Cheng, B. Wang, Q. Feng, X. Zhang and M. Chen, *Bioresour. Technol.*, 2021, **340**, 125696.
33 T. Chen, Y. X. Zhang, H. T. Wang, W. J. Lu, Z. Y. Zhou, Y. C. Zhang and L. L. Ren, *Bioresour. Technol.*, 2014, **164**, 47–54.
34 J. Li, B. Li, H. Huang, N. Zhao and L. Cao, *Sci. Total Environ.*, 2020, **714**, 136839.
35 F. F. Ma, B. W. Zhao, J. R. Diao, J. K. Zhong and A. B. Li, *Environ. Sci.*, 2015, **36**, 1678–1685.
36 H. Y. Luo, Y. J. Wang, X. P. Wen, S. L. Cheng, J. Li and Q. T. Lin, *Sci. Total Environ.*, 2020, **766**, 142618.
37 B. T. Li, F. Y. Jing, Z. Q. Hu, Y. X. Liu and D. B. Guo, *J. Saudi Chem. Soc.*, 2021, **25**, 101213.
38 J. Q. Liang, Y. Lv, Y. Lu, X. H. Wang, M. Zheng and K. N. Xu, *Environ. Eng.*, 2020, **38**, 89–94.
39 M. Li, Z. Zhang, Z. Li and H. Wu, *Ecol. Eng.*, 2020, **149**, 105792.
40 D. Liu, Z. B. Huang, S. H. Men, H. Zhen and C. R. Wnag, *Water Sci. Technol.*, 2019, **79**, 2175–2184.
41 P. M. Melia, R. Busquets, P. S. Hooda, A. B. Cundy and S. P. Sohi, *Sci. Total Environ.*, 2019, **675**, 623–631.
42 J. K. Njuguna, R. B. Zhang, Y. Li, X. J. Wang and J. F. Zhao, *Acta Sci. Circumstantiae*, 2018, **38**, 4383–4390.
43 Y. H. Shen, L. L. Zhuang, J. Zhang, J. L. Fan, T. Yang and S. Sun, *Chem. Eng. J.*, 2019, **359**, 706–712.
44 L. Y. Shi, A. L. Wei, K. D. Xue, X. Q. Zheng and H. Gao, *Environ. Pollut. Control*, 2017, **39**, 1077–1081.
45 M. M. Zhi, P. F. Wang, Z. Y. Hou, J. Cao and Y. Z. Yang, *Environ. Sci.*, 2019, **40**, 669–676.
46 Y. Zhu, Q. B. Xiao, Y. L. Xi, D. Gao, Y. X. Wang, J. Du and X. M. Ye, *Ecol. Environ. Sci.*, 2020, **29**, 1897–1903.
47 O. C. Hai, X. S. Guo, B. Y. Xiao, X. Wang and J. X. Liu, *Acta Sci. Circumstantiae*, 2017, **37**, 213–218.